analytical chemistry

Article

pubs.acs.org/ac

Measurement of Gas and Aerosol Phase Absorption Spectra across the Visible and Near-IR Using Supercontinuum Photoacoustic Spectroscopy

James G. Radney and Christopher D. Zangmeister*

Material Measurement Laboratory, National Institute of Standards and Technology, Gaithersburg, Maryland 20899, United States

Supporting Information

ABSTRACT: We demonstrate a method to measure the absorption spectra of gas and aerosol species across the visible and near-IR (500 to 840 nm) using a photoacoustic (PA) spectrometer and a pulsed supercontinuum laser source. Measurements of gas phase absorption spectra were demonstrated using $H_2O_{(g)}$ as a function of relative humidity (RH). The measured absorption intensities and peak shapes were able to be quantified and compared to spectra calculated using the 2012 High Resolution Transmission (HITRAN2012) database. Size and mass selected nigrosin aerosol was used to measure absorption spectra across the visible and near-IR. Spectra were measured as a function of aerosol size/mass and show good agreement to Mie theory calculations. Lastly, we measured the broadband absorption spectrum of flame generated soot aerosol at 5% and 70% RH. For the high RH case, we are able to quantifiably separate the soot and water absorption contributions. For soot, we observe an enhancement in the mass specific absorption cross section ranging from 1.5 at 500 nm ($p < 0.01$) to 1.2 at 840 nm ($p < 0.2$) and a concomitant increase in the absorption Ångström exponent from 1.2 ± 0.4 (5% RH) to 1.6 ± 0.3 (70% RH).

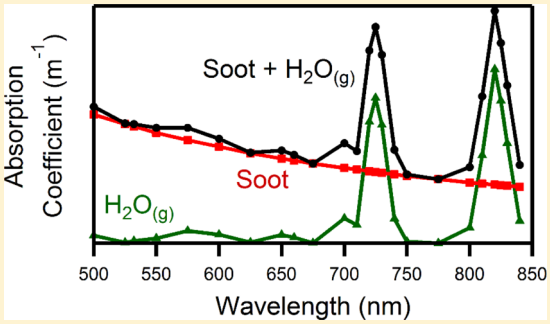

Atmospheric trace gases and aerosols directly affect the Earth's radiation budget through the absorption of solar radiation.[1] Absorption by most gases is weak in the visible and near-IR portion of the solar transmission window. This is also the wavelength region where aerosols exert their greatest direct effect, as particle size is comparable to the wavelength of light and the number concentration is sufficiently high.[2] Measurement of aerosol absorption is challenging when compared to gas-phase measurements. Aerosols can have large scattering cross sections, negating the use of transmission spectroscopies that are typically employed for measurement of gas-phase absorption. Thus, alternative techniques are required to directly measure absorption.

Photoacoustic spectroscopy (PAS) represents one method to measure the absorption of gas and/or aerosol-phase species *in situ*.[3] A light source is modulated at an acoustic frequency (10 to 10^4 Hz) where light absorption and the concomitant thermal relaxation lead to the generation of a pressure wave at the carrier frequency that is detected using a microphone. PAS can utilize either a nonresonant or resonant acoustic cavity, and depending upon the nature of the sample, both have their advantages and disadvantages.[3b] For a resonant acoustic cavity, the acoustic pressure generated ($\bar{p}$) at the resonance frequency f_0 depends on the absorption coefficient (α_{abs}), the incident optical power (W), the resonator length (L), and volume (V)

$$\bar{p} = \frac{\gamma - 1}{\beta_p T} \frac{QGL}{2\pi f_0 V} R \alpha_{abs} W \tag{1}$$

where T is the temperature.[4] The absorption coefficient (α_{abs}) represents the fractional loss in light intensity per unit propagation distance (we use units of inverse meters, m^{-1}) and depends upon the particle's absorption cross section (C_{abs}) and number density (N) through

$$\alpha_{abs} = C_{abs} N \tag{2}$$

The terms G and R in eq 1 represent the dimensionless overlap integral that accounts for the shape of the resonator and the relative response factor, respectively, which we assume to be 1. The measured signal is also dependent upon the bath gas in which the measurement, taking place through the ratio of the isobaric and isochoric specific heats, is given by the term γ (γ = 1.4 in air).[3c] Since measurements are performed in a resonant acoustic cavity, the quality factor (Q) represents the ratio of the resonance frequency (f_0) to the half width (g) of the resonance

$$Q = \frac{f_0}{2g} \tag{3}$$

The speed of sound is a function of temperature and gas composition causing the resonance frequency to display a similar dependence. Acoustic resonators with high Q are achievable (>1000),[5] but moderate values for Q (20 to 30) are

Received: April 23, 2015
Accepted: June 22, 2015
Published: June 22, 2015

DOI: 10.1021/acs.analchem.5b01541
Anal. Chem. 2015, 87, 7356−7363

preferred to reduce resonance sensitivity to changes in ambient conditions.[6] By measuring resonator response at multiple frequencies (f) around the resonance frequency, values for f_0 and g can be determined by fitting the resonance response function[4,5c]

$$u + iv = \frac{ifA}{(f_0 + g)^2 - f^2} + B + C(f - \bar{f}) \quad (4)$$

where u and v are the real and imaginary component of the acoustic response, A is the complex amplitude, and $\bar{f}$ is the midpoint frequency between the highest and lowest measured frequency. The terms B and C are adjusted background parameters that account for the tails of other modes, frequency dependence of the transducers, cross talk, etc. Since many of the terms in eq 1 are constants, this expression can be simplified and rearranged to solve for α_{abs}

$$\alpha_{abs} = \frac{P_m}{\beta_m} \frac{1}{C_c W_{pp}} \quad (5)$$

where P_m, β_m, and C_c are the microphone voltage measured at the resonant frequency, the microphone sensitivity, and the cell constant.[7] Since the acoustic response (P_m) contains both real and imaginary components, phase sensitive detection is required. In practice, this can be done by taking the fast Fourier transformation[8] of the measured data in time or using a lock-in amplifier.[4,8a,9]

Measured PAS signal is proportional to the peak-to-peak source intensity, so it is advantageous to use high intensity light sources. Gas-phase measurements can be performed at longer wavelengths (specifically the telecom region) where fiber amplifiers can achieve Watt peak powers.[10] Most aerosol experiments are limited to data collection at a few discrete laser wavelengths (4 or less) where sufficient power is available (i.e., λ = 266 nm,[11] 355 nm,[11,12] 404 nm,[7,13] 532 nm,[8a,b,11,13b,14] 660 nm,[13b,15] 685 nm,[8a] 870 nm[13a] 1047 nm,[14] and 1064 nm[11]), minimizing resolution across the absorption spectrum. Each discrete laser wavelength often requires its own acoustic resonator, complicating the experimental setup. For low power measurements, temporal resolution is sacrificed: 48 s wavelength^{-1} in Reed et al.[10] for measurement of CO_2 versus 5 min wavelength^{-1} presently.

The narrow spectral features of gas-phase species allow multiple species to be simultaneously measured in a spectral region spanning only a few wavenumbers. Aerosols are broadband absorbers spanning the UV to near-IR, requiring significantly greater spectral coverage to adequately capture a full absorption spectrum. Broadband measurements using an Hg arc lamp,[9a] an optical parametric oscillator,[8c] or a supercontinuum laser[16] to collect PAS spectra using a single acoustic resonator have been demonstrated. The Hg lamp of Wiegand et al.[9a] is capable of providing 44 to 382 mW of power at 8 discrete wavelengths spanning 300 to 700 nm with bandwidths ranging from 8 to 64 nm at 20 s wavelength^{-1} temporal resolution. The supercontinuum laser of Sharma et al.[16] provided 16 to 86 mW of power at 5 discrete wavelengths from 417 to 675 nm with bandwidths ranging from 56.4 to 80 nm at 3 to 4 min wavelength^{-1}. In both of the described systems, an optical filter wheel was used for wavelength selection. The average powers of these systems are comparable to some of the discrete emission line lasers employed in other PAS systems and are larger than the ones in the present work (14 to 27 mW). However, the bandwidths employed are comparable to and larger than that used in the present work (10 to 20 nm), respectively, and the wavelength resolution is significantly less than in the present work (16 to 22 discrete wavelengths spanning 500 to 840 nm; see Supporting Information for a detailed list of peak powers and bandwidths) at a comparable temporal resolution; higher wavelength resolution is achieved here through the use of a tunable wavelength and bandwidth filter. The OPO of Haisch et al.[8c] provides less power (0.8 to 8 mJ) with comparable spectral coverage (410 to 710 nm) but provides better wavelength and temporal resolution, 150 GHz and 30 s wavelength^{-1}, respectively. They also achieve a 2.5 × 10^{-7} m^{-1} limit of detection, comparable to some of the discrete emission line laser systems and nearly 100 times lower than the values quoted in the present work (see Supporting Information), by using a microphone with lower noise and higher sensitivity than the one used in this work.

Many greenhouse gases exhibit lifetimes on the order of years so their concentration can be considered globally distributed.[1a] Radiative transfer models for gases have been developed that can parametrize the strength of gas phase absorption based upon both temperature and pressure.[17] The parametrization of aerosols in radiative transfer models is more complex due to their diverse physical, chemical, and morphological properties and short atmospheric lifetimes. From a first-principles approximation, particle absorption can be calculated using either: (1) a particle size distribution, number concentration, mass density, and refractive index[18] or (2) a wavelength dependent and size independent mass-specific absorption cross section (MAC, in units of m^2 g^{-1}) and particle mass concentration (M, in units g m^{-3}).[19] The first set of assumptions may cause prediction errors due to uncertainties in particle density. However, the dependence of spectral shape on particle size will be captured. Under the second set of assumptions, any spectral shape dependence on particle size will be lost as absorption is directly calculated from MAC. A recent modeling study by Moosmüller et al.[20] demonstrated spectral shape dependence on particle size for spherical brown carbon particles (BrC). Measurements of aerosol light absorption in the Amazon basin alluded to size dependent optical properties; however, changes in physiochemical composition could not be ruled out, disallowing a definitive assignment.[21] Other recent field-based investigations have observed aerosol absorption changes with size but assigned the spectral variation to changes in chemical composition discounting any size dependent optical properties.[22] To date, measurements of the spectral dependence of chemically similar aerosols as a function of size have yet to be experimentally demonstrated.

In this investigation, we describe a technique to collect a photoacoustic (PA) absorption spectra across the visible and near-IR (500 to 850 nm) for both gas and aerosol phase species. We first demonstrate the method by comparing measured absorption spectra of $H_2O_{(g)}$ to spectra calculated using the 2012 High Resolution Transmission (HITRAN2012) database.[23] We then measure the MAC of aerosolized nigrosin, a highly documented absorbing dye,[9a,24] to show the first experimentally measured dependence of aerosol spectral shape on particle size and mass. Finally, we demonstrate that it is possible to quantitatively measure both gas- and aerosol-phase absorption spectra simultaneously using a broadband source and that the spectral contributions from each can be separated.

DOI: 10.1021/acs.analchem.5b01541
Anal. Chem. 2015, 87, 7356−7363

MATERIALS AND METHODS

The experimental setup used to determine water vapor and/or aerosol absorption spectra is shown in Figure 1.

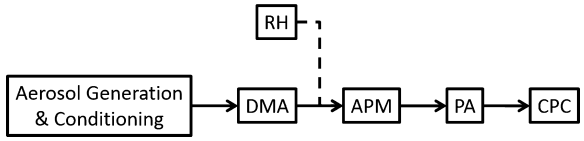

Figure 1. Block diagram of the experimental setup used for absorption spectral measurements. Acronyms: humidity generator (HG), differential mobility analyzer (DMA), aerosol particle mass analyzer (APM), photoacoustic spectrometer (PA), and condensation particle counter (CPC).

Absorption Spectrum Measurement. For a detailed description of the determination of aerosol absorption coefficients by photoacoustic spectroscopy, the reader is directed to Arnott et al.;[8a] Lack et al.;[8b] Ajtai et al.;[9b] or Gillis et al.[4] Here, only a brief description of the PA, as shown in Figure 2, for the measurement of absorption spectra, relative to a single wavelength PA used in previous investigations, will be provided.[7,25]

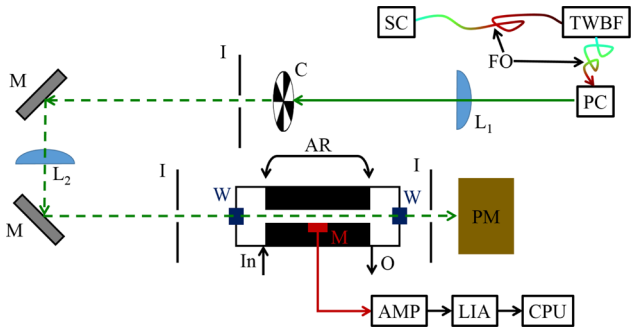

Figure 2. Schematic of the photoacoustic instrument used. Acronyms: supercontinuum laser (SC), tunable wavelength and bandwidth filter (TWBF), parabolic collimator (PC), fiber optics (FO), focusing lenses (L_1, L_2), mechanical chopper (C), iris (I), mirror (M), window (W), microphone (M), acoustic resonator (AR), power meter (PM), aerosol inlet (In), outlet (O), low-noise preamplifier (AMP), lock-in amplifier (LIA), and computer (CPU).

Wavelength selection and amplitude modulation of a supercontinuum laser (NKT Photonics SuperK Extreme EXR-15, ≈5.5 W over 475 nm to 2.5 μm, ≈1.5 W over 475 to 700 nm, 78 MHz repetition rate, 650 ps pulse width)[26] was performed using a tunable wavelength and bandwidth filter (NKT Photonics SuperK Varia, output 475 to 850 nm) and mechanical chopper (ThorLabs MC-2000 with MC1F30 blade) driven by a function generator (Stanford Research Systems DS345), respectively. The tunable wavelength and bandwidth filter has a minimum bandwidth of <10 nm, a maximum bandwidth of 100 nm, and >50 dB of out of band suppression and is able to change wavelengths at greater than 10 nm s^{-1} with an absolute wavelength accuracy and repeatability of ±5 nm and <0.02 nm, respectively. The input and output of the tunable wavelength and bandwidth filter are fiber coupled to the supercontinuum laser and a protected silver reflective collimator (ThorLabs RC04FC-P01), respectively. The laser then travels in free space through the chopper and the PA cell. An iris is situated ≈25 mm behind the chopper, and two more irises are situated ≈25 mm before and after the resonator to remove stray light from the collimator, light diffracted by the chopper and light reflected by the face of the power meter, respectively. At this aperture diameter, the irises serve to only remove stray light and do not affect the total power transmitted, although the beam width is a function of wavelength (see Supporting Information Figure S1). Filter bandwidth was chosen such that the total laser power reaching the PA was a minimum of 14 mW, as measured by a calibrated power meter (Newport, model 2931-C with 91D-SL-OD3 detector) situated at the resonator exit. For wavelengths where the bandwidth required to obtain 14 mW would have been less than 10 nm, the bandwidth was set to 10 nm. The average power, bandwidth, and corresponding limits of detection can be seen in Table S1 of the Supporting Information. The laser power was chosen as a compromise between: (1) the reduction of measurement noise via maximizing laser power, (2) minimizing bandwidth for adequate spectral resolution, (3) minimizing the effect of the nonlinear and nonuniform per nm power density of the supercontinuum laser, and (4) compensating for the output profile of the tunable wavelength and bandpass filter (see Supporting Information Figure S2). This method is in contrast to a similar supercontinuum photoacoustic spectrometer developed by Sharma et al.[16] where the focus was on sensitivity at the expense of spectral resolution (average bandwidth of ≈66 nm).

The microphone signal was conditioned with a low noise preamplifier (Stanford Research Systems, model SR560) set to 6 dB/octave roll-off below 300 Hz and above 3000 Hz. The conditioned microphone signal was passed to a lock-in amplifier (LIA, Stanford Research Systems, model SR830, τ = 10 ms). The in-phase (x) and quadrature (y) components of the LIA and the analog output of the power meter were then sampled at 100 kHz for 1 s using National Instruments BNC-2120 and PCI-6281 data acquisition boards and analyzed using LabView 8.6 virtual instruments using custom written code. Power meter data was analyzed by calculating the power spectrum using a fast Fourier transformation (FFT). From the power spectrum, the RMS voltage at the modulation frequency (V_{RMS}) was retained for further analysis while the remainder of the data was discarded. This RMS voltage was multiplied by the power meter's range setting at each wavelength and $\sqrt{8}$ to obtain the peak-to-peak laser power (W_{pp}). LIA data was simply averaged. Absorption coefficients were then calculated from

$$\alpha_{abs} = \frac{\sqrt{(x - x_0)^2 + (y - y_0)^2}}{C_c \beta_m W_{pp}} \quad (6)$$

where the pairs x and y and x_0 and y_0 are the LIA voltages while measuring aerosols or LIA signal with the laser off, respectively. The terms C_c and β_m represent the calculated cell constant of the acoustic resonator and the microphone sensitivity as measured using a constant-amplitude sound source, respectively;[7] presently, $C_c\beta_m$ = 0.187 V m W^{-1}. In total, 30, 1 s samples were analyzed and averaged. The 30 s averages were binned and averaged to 5 min. The limit of detection (LOD) at this averaging time, defined as three times the background deviation, was calculated using an Allan variance and determined to be 9.6 × 10^{-8} W m^{-1} independent of wavelength; the corresponding noise equivalent power is 2.4 × 10^{-9} W m^{-1} $Hz^{-1/2}$ at the nominal f_0 of 1640 Hz. Wavelength regions were randomized at the start of each experiment to reduce systematic errors.

DOI: 10.1021/acs.analchem.5b01541
Anal. Chem. 2015, 87, 7356−7363

Water Vapor Absorption Spectra. Moist air was generated using a humidity generator (InstruQuest, Inc. HumiSys HF) at multiple relative humidity values. The absorption spectrum was measured using the PA at 15 wavelength sections spanning 625 to 825 nm. Measurements with significant amounts of water vapor had an additional 7 wavelengths sections added around 725 and 825 nm to resolve the absorption bands located there. The relative humidity (RH) of the air stream was monitored by a RH and temperature sensor (Air Chip Technology HygroClip2) that was calibrated using a chilled mirror hygrometer (Edgetech Instruments DewMaster). Absorption spectra were calculated using HITRAN2012 with a resolution of 0.05 cm^{-1}.[23]

Nigrosin Generation and Conditioning. Nigrosin (Sigma-Aldrich, water-soluble) aerosols were generated from 2 mg mL^{-1} solution using a liquid jet cross-flow atomizer (TSI 3076, 30 psig). A portion of the generated flow (0.5 L min^{-1}) was sampled for conditioning and measurement while the excess flow (≈1.5 L min^{-1}) was exhausted to a fume hood. Aerosols were conditioned by passing the stream through a large diameter Nafion dryer (PermaPure MD-700-48F-3), a pair of diffusion dryers (TSI 3062), and a tube furnace (Lindberg-Blue Mini-Mite) at 150 °C. The relative humidity (RH) of the air stream exiting the dryers was monitored using a RH and temperature sensor and was typically <10 ± 2% RH prior to optical measurement. The desiccant was replaced when the air stream was >15% RH. The dry aerosol was then size-selected using a differential mobility analyzer (DMA, TSI 3080 Electrostatic classifier with 3081L column) and mass-selected using an aerosol particle mass analyzer (APM, Kanomax 3601). Particle number concentration was measured using a condensation particle counter (CPC, TSI 3775). Coupled to the PA absorption measurement, the observables measured by the APM and CPC of mass (m_p) and number density (N), respectively, allow for the calculation of aerosol MAC through

$$\mathrm{MAC} = \frac{\alpha_{abs}}{N m_p} = \frac{C_{abs}}{m_p} \tag{7}$$

The DMA is present to allow for isolation of the +1 charged particle of interest.[25]

Solution Absorption Spectra. The absorption spectra of 5×10^{-3} mg mL^{-1} nigrosin solution under acidic, neutral, and basic conditions were measured from 500 to 850 nm with a 4 nm slit width using a PerkinElmer Lambda Bio 20.

Soot Generation. Soot was generated using a Santoro diffusion flame[27] with ethylene fuel. Soot was aspirated into a dry, HEPA-filtered carrier air stream via a sampling tube located 5 cm above the centerline of the burner. No further conditioning of the soot was performed prior to size selection by the DMA. Flows from the humidity generator and DMA were merged prior to the APM for the measurement of soot at elevated humidity.

RESULTS AND DISCUSSION

Water Vapor Absorption Spectrum. The water vapor absorption spectrum from 625 to 840 nm is shown in Figure 3 for a relative humidity of 5% (black, $x_{H_2O} = 1.28 \times 10^{-3} \pm 5 \times 10^{-5}$), 20% (red, $x_{H_2O} = 5.14 \times 10^{-3} \pm 8 \times 10^{-5}$), 40% (green, $x_{H_2O} = 1.03 \times 10^{-2} \pm 1 \times 10^{-4}$), 60% (cyan, $x_{H_2O} = 1.54 \times 10^{-2} \pm 2 \times 10^{-4}$), and 80% (blue, $x_{H_2O} = 2.05 \times 10^{-2} \pm 2 \times 10^{-4}$); x_{H_2O} represents the mole fraction water at a given temperature and pressure. The temperature of all experiments was 296.7 ± 0.1 K. The error bars correspond to the 2σ measurement uncertainty. The absorption spectrum of $H_2O_{(g)}$ was calculated using Voigt profiles based on calculated collisional and Doppler widths determined from HITRAN 2012[23] line parameters at 10% RH at 296 K with a resolution of 0.05 cm^{-1}; this corresponds to a nominal $H_2O_{(g)}$ mole fraction of 2.76×10^{-3} in 1.01325×10^5 Pa (1 atm) of air (see Supporting Information for all calculated spectra). To account for the bandwidth and power density of the laser, absorption coefficients were calculated as

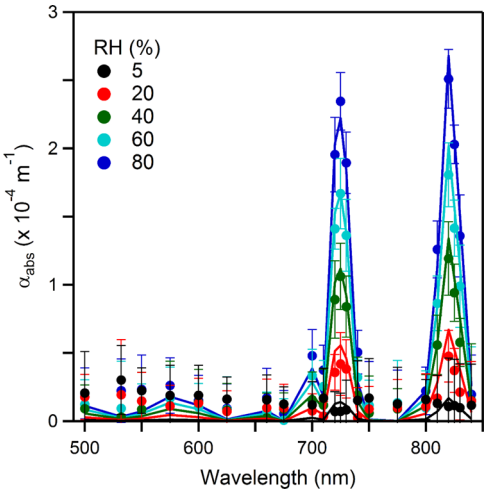

Figure 3. Absorption spectrum of water vapor at 5% (black), 20% (red), 40% (green), 60% (cyan), and 80% (blue) relative humidity. Error bars correspond to 2σ of measurement uncertainty. Solid lines correspond to the calculated absorption spectrum from HITRAN for the specified bandwidths.

$$\alpha_{abs} = \frac{\int S(\lambda) P(\lambda)\, d\lambda}{\int P(\lambda)\, d\lambda} \tag{8}$$

where $S(\lambda)$, $P(\lambda)$, and $d\lambda$ are the signal intensity and power at a given wavelength (λ) and the spacing between sequential wavelengths, respectively. Power density was measured for wavelength regions ≥600 nm using an optical spectrum analyzer (Yokogawa AQ6370D; see Supporting Information Figures S2 and S4 though S22). Across the set of wavelengths where the measured absorption is above the limit of detection, the average absolute value of the relative error is <16%. To account for microphone response as a function of H_2O vapor, absorption was measured at the peak wavelengths of 725 and 820 nm, but no significant deviations from linearity were observed (see Supporting Information Figure S23). Absorption is also expected from water dimers[28] and $O_{2(g)}$ in the near-IR, neither of which were accounted for in the model described above; $O_{2(g)}$ has an absorption peak at 775 nm of 3.5×10^{-5} m^{-1}. The agreement between measured data and calculated values suggests that $H_2O_{(g)}$ can be used as a calibration source for PAS in the near-IR.

Nigrosin Aerosol Mass-Specific Absorption Spectrum. Nigrosin has been previously used as a model for absorbing atmospheric aerosol[9a,24] as it forms spherical particles[8b] that absorb strongly across the visible region, with a well-defined peak (solution absorption peak at ≈550 nm) making it an ideal material to measure an aerosol absorption spectrum. Utilizing a broadband source with sufficient resolution allows for relatively

DOI: 10.1021/acs.analchem.5b01541
Anal. Chem. 2015, 87, 7356−7363

small variations in the spectral shape to be resolved. By selecting aerosol with known size and mass, the data can be quantitatively compared to Mie theory.

The measured nigrosin aerosol mass specific absorption spectrum for two mobility diameter and mass combinations, 250 nm and 1.04×10^{-14} g and 450 nm and 5.80×10^{-14} g, are shown in Figure 4 as red squares and green triangles,

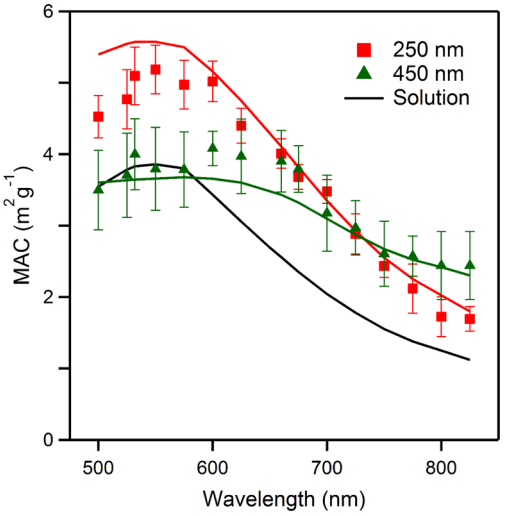

Figure 4. Measured nigrosin mass specific absorption (MAC) spectrum for 250 and 450 nm mobility diameters; red squares and green triangles, respectively. The solid black line corresponds to the absorption spectrum of a 7.53×10^{-2} mg mL^{-1} solution. Solid red and green lines correspond to calculated Mie theory values for the corresponding sizes.

respectively; the solid red and green lines correspond to MAC values calculated using Mie theory and a particle density of 1.34 g cm^{-3} (average from mass distribution fits; see Supporting Information for density measurements and refractive index determination as a function of wavelength). The solid black line corresponds to the measured mass-specific absorption spectrum of a 5.0×10^{-3} mg mL^{-1} solution in base (pH > 10). The error bars in MAC represent the 2σ measurement uncertainty, as calculated from propagation of uncertainty in the measured absorption, laser power, mass, and number concentration. A total of 15 wavelength regions were used, versus using 22 for water vapor, spanning 500 to 825 nm. In this measurement, less resolution was required due to the low RH (<10%) and the absence of fine structure as observed with the $H_2O_{(g)}$ measurement. As can be seen from Figure 4, good agreement between the calculated and measured values is obtained for all wavelengths measured with an average absolute deviation of ≈7%. Uncertainties are greatest toward the blue side of the spectrum and are most likely a result of using extinction data to determine the refractive index[29] and extrapolating these values across the entire spectrum (see Supporting Information for full discussion on how refractive index values were obtained). To our knowledge, these nigrosin absorption spectra represent the first well-resolved quantitative experimental demonstrations on the chemically similar size dependence of aerosol absorption spectra using a photoacoustic spectrometer. Other measurements of aerosol light absorption have alluded to size dependent optical properties; however, in each instance, changes in physiochemical composition were attributed to the size-dependent optical properties.[21,22]

Previous investigations have attempted to compare the measured aerosol absorption spectrum to the same material in solution.[9a,30] However, both Mie theory and the data presented here demonstrate that care should be taken with comparison between solution- and aerosol-phase absorption measurements as the spectral shape and MAC are a function of aerosol size. Instead, we recommend that the wavelength dependent refractive indices be used for comparison between solution and aerosolized material as Mie theory calculations will capture the spectral size dependence.

Soot and Water Vapor Absorption Spectrum. As a demonstration of the utilization of the broadband photoacoustic technique over a wide spectral region, we measured the absorption spectrum of soot generated from a Santoro diffusion flame. Data were collected at both low (5%) and elevated (70%) RH as shown in Figure 5a as the black circles and red

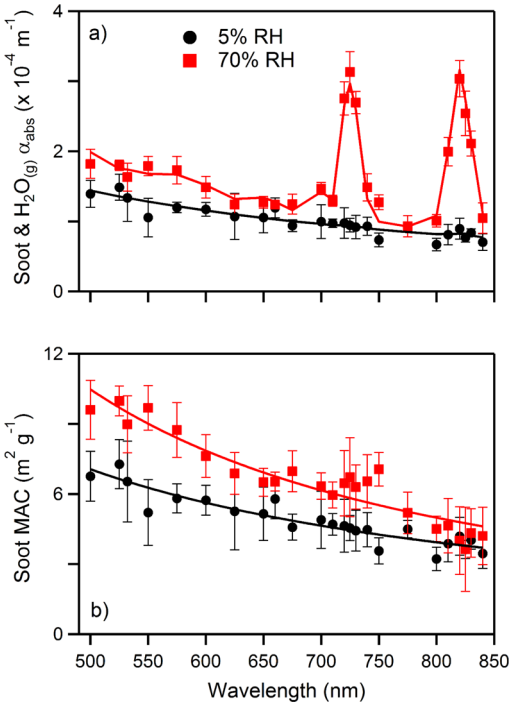

Figure 5. (a) Measured absorption spectrum of size and mass-selected soot at 5% (black circles) and 70% RH (red squares). (b) Soot mass specific absorption spectrum after removal of $H_2O_{(g)}$ absorption. Solid lines are fits to the data using eqs 12 and 11 in a and b, respectively. Error bars represent 2σ of measurement uncertainty.

squares, respectively. The temperature of all experiments was 297.4 ± 0.2 K. The total measured absorption contains contributions from both the soot and $H_2O_{(g)}$.

$$\alpha_{abs} = \alpha_{soot} + \alpha_{H_2O_{(g)}} \quad (9)$$

The absorption by water vapor can be calculated using the power-weighted absorption coefficients ($\alpha_{H2O(g)}$) determined from HITRAN and the mole fraction water (x_{H_2O}).

$$\alpha_{H_2O_{(g)}} = \frac{x_{H_2O}}{2.73 \times 10^{-3}} \times \alpha_{H_2O_{(g)}}(2.73 \times 10^{-3}) \quad (10)$$

The 2.73×10^{-3} term represents the mole fraction of $H_2O_{(g)}$ at 10% RH and STP. The absorption contribution from the aerosol is simplified by assuming the absorption is described by

DOI: 10.1021/acs.analchem.5b01541
Anal. Chem. 2015, 87, 7356−7363

a single power law expression, the absorption Ångström exponent (AAE)[20] where

$$\mathrm{MAC}_\lambda = k_0\left(\frac{\lambda}{500\,\mathrm{nm}}\right)^{-\mathrm{AAE}} \tag{11}$$

Since particle mass and number concentration are also known, it follows from eq 8 that

$$\alpha_{\mathrm{abs}} = N \times m_{\mathrm{p}} \times k_0\left(\frac{\lambda}{500\,\mathrm{nm}}\right)^{-\mathrm{AAE}} + \frac{x_{\mathrm{H_2O}}}{2.73 \times 10^{-3}} \times \alpha_{\mathrm{H_2O_{(g)}}}(2.73 \times 10^{-3}) \tag{12}$$

The fitting procedure was applied for each RH in Figure 5a, as shown by the solid lines. From the fitted data, it is possible to extract the soot absorption contribution from the total absorption spectrum and calculate the soot MAC under both conditions. The RH calculated from the fit, MAC at λ = 500 nm, and the AAE are shown in Table 1; uncertainties are 2σ.

Table 1. Fit Coefficients for Low and High RH Absorption Spectra with Soot

$\mathrm{RH_{set\ point}}$ (%)	$\mathrm{RH_{calc}}$ (%)	k_0 ($\mathrm{m^2\ g^{-1}}$)	AAE
5	1 ± 4	7.0 ± 0.4	1.2 ± 0.4
70	68 ± 8	10.4 ± 0.7	1.6 ± 0.3

Good agreement is obtained between the RH measured by the probe and the calculated RH. For comparison, the low RH MAC value of 5.2 ± 1.4 $\mathrm{m^2\ g^{-1}}$ at λ = 550 nm is lower than the widely referenced Bond et al.[31] and Bond and Bergstrom[32] value of 7.5 $\mathrm{m^2\ g^{-1}}$ but is higher than our previous measurements of 5.69 ± 0.83 $\mathrm{m^2\ g^{-1}}$ at λ = 405 nm using a similar setup[25b] (extrapolation of our current value to λ = 405 nm yields 9.0 $\mathrm{m^2\ g^{-1}}$), likely from a lower organic fraction in the soot used in this investigation.

The measured data show that both MAC and AAE of the soot are a function of RH, with higher values being measured at higher RH. The MAC enhancement is spectrally dependent ranging from 1.5 at 500 nm ($p < 0.01$) to 1.2 at 840 nm ($p < 0.2$) causing a concomitant enhancement in the AAE from 1.2 ± 0.4 to 1.6 ± 0.3. The measured enhancement can be attributed to a thin surface coating of water. The magnitude of a particle's enhancement is likely a function of the wavelength dependent dry particle absorption cross section, as discussed in previous modeling results.[33] Importantly, simulations have shown that a thin coating of water on soot, regardless of its thickness, leads to absorption enhancement,[34] although previous PAS investigations at RH ≥ 70% have measured an absorption decrease.[35] Attenuation of the absorption signal in PAS at high RH has been rationalized by thermal transfer to the water layer and energy loss through vaporization into the gas phase.[36] It is likely that water evaporation contributes to the measured acoustic signal due to a pressure increase, but the offset in energy transferred to the gas phase from the latent heat of vaporization more than counterbalances this effect. Signal reduction from coating vaporization at high RH is a limitation of PAS and is a challenge to decouple the effect of the coating from the intrinsic absorption cross section. It is important to note that experiments presented here use an ultrafast, pulsed laser source (78 MHz repetition rate and 650 ps pulse duration, respectively), which we posit circumvents coating vaporization as the particle thermal relaxation is faster than the evaporation rate of water for soot. This is in contrast to previous studies that utilize continuous-wave (CW) lasers, where particle heating and cooling occur at the acoustic period (≈3 orders of magnitude slower than the pulsed laser used in this study) thereby allowing evaporation to occur and reducing the apparent cross section.[35] The effect of utilizing an ultrafast pulsed laser source was investigated by measuring soot using a CW source at identical time-averaged laser power and wavelength (660 nm). Absorption cross sections were measured at 5% and 70% RH. The measured absorption cross sections for the CW laser were comparable within measurement uncertainty at both RH values while the pulsed laser source was enhanced by 21% at 70% RH. The presented data suggest that through judicious choice of pulse duration and/or source duty cycle one may be able to negate signal dampening in PAS of humidified environments. More detailed investigations are currently underway to fully understand these observations.

The technique described is able to quantitatively measure the absorption spectrum of gas and aerosol phase species across the visible and near-IR and allows for the decoupling of each phase's contribution to the total signal. We used the technique to measure the absorption spectrum of water vapor and compared that to the spectrum calculated using HITRAN2012. We then demonstrated the ability to quantify aerosol MAC by measuring two size and mass selected particle distributions to show that the spectral shape is a function of particle size, consistent with previous modeling results.[20] Unlike previous measurements where particle composition was asserted to be the driving force for changes in MAC and spectral shape,[21,22] the observed changes presented have arisen solely from changes in particle size. We conclude by demonstrating the ability to decouple absorption signals from a gas and aerosol sample and the ability to measure soot absorption enhancement at high RH by utilizing a pulsed laser source.

■ ASSOCIATED CONTENT

Supporting Information

Further details related to the characterization of the supercontinuum laser for photoacoustic measurements, integrated water vapor absorption coefficients at 10% RH and STP (including plots of spectra), microphone responsivity to RH, and significant discussion on the determination of nigrosin's wavelength dependent refractive indices are included. The Supporting Information is available free of charge on the ACS Publications website at DOI: 10.1021/acs.analchem.5b01541.

■ AUTHOR INFORMATION

Corresponding Author

*E-mail: cdzang@nist.gov. Phone (301) 975-8709.

Author Contributions

The manuscript was written through contributions of all authors. All authors have given approval to the final version of the manuscript.

Notes

The authors declare no competing financial interest.

■ ACKNOWLEDGMENTS

Special thanks to Joseph Hodges and Keith Gillis at the National Institute of Standards and Technology for assistance with the calculation of H_2O vapor absorption spectra using

DOI: 10.1021/acs.analchem.5b01541
Anal. Chem. 2015, 87, 7356−7363

HITRAN and useful discussions about the physics of acoustic responses, respectively.

REFERENCES

(1) (a) Hartmann, D. L.; Klein Tank, A. M. G.; Rusticucci, M.; Alexander, L. V.; Brönnimann, S.; Charabi, Y.; Dentener, F. J.; Dlugokencky, E. J.; Easterling, D. R.; Kaplan, A.; Soden, B. J.; Thorne, P. W.; Wild, M.; Zhai, P. M. In *Climate Change 2013: The Physical Science Basis. Contribution of Working Group I to the Fifth Assessment Report of the Intergovernmental Panel on Climate Change*; Stocker, T. F., Qin, D., Plattner, G.-K., Tignor, M., Allen, S. K., Boschung, J., Nauels, A., Xia, Y., Bex, V., Midgley, P. M., Eds.; Cambridge University Press: Cambridge, United Kingdom and New York, NY, USA, 2013; pp 159−254; DOI: 10.1017/CBO9781107415324.008. (b) Boucher, O.; Randall, D.; Artaxo, P.; Bretherton, C.; Feingold, G.; Forster, P.; Kerminen, V.-M.; Kondo, Y.; Liao, H.; Lohmann, U.; Rasch, P.; Satheesh, S. K.; Sherwood, S.; Stevens, B.; Zhang, X. Y. In *Climate Change 2013: The Physical Science Basis. Contribution of Working Group I to the Fifth Assessment Report of the Intergovernmental Panel on Climate Change*; Stocker, T. F., Qin, D., Plattner, G.-K., Tignor, M., Allen, S. K., Boschung, J., Nauels, A., Xia, Y., Bex, V., Midgley, P. M., Eds.; Cambridge University Press: Cambridge, United Kingdom and New York, NY, USA, 2013; pp 571−658, DOI: 10.1017/CBO9781107415324.016.

(2) Finlayson-Pitts, B. J.; Pitts, J. N., Jr. *Chemistry of the upper and lower atmosphere: Theory, Experiments and Applications*; Academic Press: San Diego, CA, 2000; p 969.

(3) (a) Rosencwaig, A. *Photoacoustics and Photoacoustic Spectroscopy*; John Wiley & Sons: New York, NY, 1980; Vol. *57*, p 309. (b) Haisch, C. *Meas. Sci. Technol.* **2012**, *23*, 012001. (c) Miklós, A.; Hess, P. *Anal. Chem.* **2000**, *72*, 30 A−37 A.

(4) Gillis, K. A.; Havey, D. K.; Hodges, J. T. *Rev. Sci. Instrum.* **2010**, *81*, 064902−0649013.

(5) (a) Schäfer, S.; Miklós, A.; Pusel, A.; Hess, P. *Chem. Phys. Lett.* **1998**, *285*, 235−239. (b) Schäfer, S.; Miklós, A.; Hess, P. *Appl. Opt.* **1997**, *36*, 3202−3211. (c) Moldover, M. R.; Trusler, J. P. M.; Edwards, T. J.; Mehl, J. B.; Davis, R. S. *Phys. Rev. Lett.* **1988**, *60*, 249−252.

(6) Miklos, A.; Hess, P.; Bozoki, Z. *Rev. Sci. Instrum.* **2001**, *72*, 1937−1955.

(7) Havey, D. K.; Bueno, P. A.; Gillis, K. A.; Hodges, J. T.; Mulholland, G. W.; van Zee, R. D.; Zachariah, M. R. *Anal. Chem.* **2010**, *82*, 7935−7942.

(8) (a) Arnott, P. W.; Moosmüller, H.; Rogers, F. C.; Jin, T.; Bruch, R. *Atmos. Environ.* **1999**, *33*, 2845−2852. (b) Lack, D. A.; Lovejoy, E. R.; Baynard, T.; Pettersson, A.; Ravishankara, A. R. *Aerosol Sci. Technol.* **2006**, *40*, 697−708. (c) Haisch, C.; Menzenbach, P.; Bladt, H.; Niessner, R. *Anal. Chem.* **2012**, *84*, 8941−8945.

(9) (a) Wiegand, J. R.; Mathews, L. D.; Smith, G. D. *Anal. Chem.* **2014**, *86*, 6049−6056. (b) Ajtai, T.; Filep, Á.; Schnaiter, M.; Linke, C.; Vragel, M.; Bozóki, Z.; Szabó, G.; Leisner, T. *J. Aerosol Sci.* **2010**, *41*, 1020−1029.

(10) Reed, Z. D.; Sperling, B.; van Zee, R. D.; Whetstone, J. R.; Gillis, K. A.; Hodges, J. T. *Appl. Phys. B: Laser Opt.* **2014**, *117*, 645−657.

(11) Ajtai, T.; Filep, A.; Kecskemeti, G.; Hopp, B.; Bozoki, Z.; Szabo, G. *Appl. Phys. A: Mater. Sci. Process.* **2011**, *103*, 1165−1172.

(12) Gyawali, M.; Arnott, W. P.; Zaveri, R. A.; Song, C.; Moosmüller, H.; Liu, L.; Mishchenko, M. I.; Chen, L. W. A.; Green, M. C.; Watson, J. G.; Chow, J. C. *Atmos. Chem. Phys.* **2012**, *12*, 2587−2601.

(13) (a) Lewis, K.; Arnott, W. P.; Moosmüller, H.; Wold, C. E. *J. Geophys. Res.: Atmos.* **2008**, *113*, D16203. (b) Lack, D. A.; Richardson, M. S.; Law, D.; Langridge, J. M.; Cappa, C. D.; McLaughlin, R. J.; Murphy, D. M. *Aerosol Sci. Technol.* **2011**, *46*, 555−568.

(14) Arnott, W. P.; Moosmüller, H.; Walker, J. W. *Rev. Sci. Instrum.* **2000**, *71*, 4545−4552.

(15) Ma, X.; Zachariah, M. R.; Zangmeister, C. D. *J. Phys. Chem. C* **2013**, *117*, 3185−3191.

(16) Sharma, N.; Arnold, I. J.; Moosmüller, H.; Arnott, W. P.; Mazzoleni, C. *Atmos. Meas. Technol.* **2013**, *6*, 3501−3513.

(17) Flato, G.; Marotzke, J.; Abiodun, B.; Braconnot, P.; Chou, S. C.; Collins, W.; Cox, P.; Driouech, F.; Emori, S.; Eyring, V.; Forest, C.; Gleckler, P.; Guilyardi, E.; Jakob, C.; Kattsov, V.; Reason, C.; Rummukainen, M. In *Climate Change 2013: The Physical Science Basis. Contribution of Working Group I to the Fifth Assessment Report of the Intergovernmental Panel on Climate Change*; Stocker, T. F., Qin, D., Plattner, G.-K., Tignor, M., Allen, S. K., Boschung, J., Nauels, A., Xia, Y., Bex, V., Midgley, P. M., Eds.; Cambridge University Press: Cambridge, United Kingdom and New York, NY, USA, 2013; pp 741−866, DOI: 10.1017/CBO9781107415324.020.

(18) (a) Feng, Y.; Ramanathan, V.; Kotamarthi, V. R. *Atmos. Chem. Phys. Discuss.* **2013**, *13*, 2795−2833. (b) Han, X.; Zhang, M.; Han, Z.; Xin, J.; Liu, X. *Atmos. Environ.* **2011**, *45*, 6576−6592.

(19) (a) Malm, W. C.; Sisler, J. F.; Huffman, D.; Eldred, R. A.; Cahill, T. A. *J. Geophys. Res.: Atmos.* **1994**, *99*, 1347−1370. (b) Park, R. S.; Song, C. H.; Han, K. M.; Park, M. E.; Lee, S. S.; Kim, S. B.; Shimizu, A. *Atmos. Chem. Phys.* **2011**, *11*, 12275−12296. (c) Roy, B.; Mathur, R.; Gilliland, A. B.; Howard, S. C. *J. Geophys. Res.: Atmos.* **2007**, *112*, D14301. (d) Basart, S.; Pay, M. T.; Jorba, O.; Pérez, C.; Jiménez-Guerrero, P.; Schulz, M.; Baldasano, J. M. *Atmos. Chem. Phys.* **2012**, *12*, 3363−3392.

(20) Moosmüller, H.; Chakrabarty, R. K.; Ehlers, K. M.; Arnott, W. P. *Atmos. Chem. Phys.* **2011**, *11*, 1217−1225.

(21) Rizzo, L. V.; Correia, A. L.; Artaxo, P.; Procopio, A. S.; Andreae, M. O. *Atmos. Chem. Phys.* **2011**, *11*, 8899−8912.

(22) (a) Utry, N.; Ajtai, T.; Filep, A.; Pinter, M.; Torok, Z.; Bozoki, Z.; Szabo, G. *Atmos. Environ.* **2014**, *91*, 52−59. (b) Filep, A.; Ajtai, T.; Utry, N.; Pinter, M. D.; Nyilas, T.; Takacs, S.; Mate, Z.; Gelencser, A.; Hoffer, A.; Schnaiter, M.; Bozoki, Z.; Szabo, G. *Aerosol Air Qual. Res.* **2013**, *13*, 49−59.

(23) Rothman, L. S.; Gordon, I. E.; Babikov, Y.; Barbe, A.; Chris Benner, D.; Bernath, P. F.; Birk, M.; Bizzocchi, L.; Boudon, V.; Brown, L. R.; Campargue, A.; Chance, K.; Cohen, E. A.; Coudert, L. H.; Devi, V. M.; Drouin, B. J.; Fayt, A.; Flaud, J. M.; Gamache, R. R.; Harrison, J. J.; Hartmann, J. M.; Hill, C.; Hodges, J. T.; Jacquemart, D.; Jolly, A.; Lamouroux, J.; Le Roy, R. J.; Li, G.; Long, D. A.; Lyulin, O. M.; Mackie, C. J.; Massie, S. T.; Mikhailenko, S.; Müller, H. S. P.; Naumenko, O. V.; Nikitin, A. V.; Orphal, J.; Perevalov, V.; Perrin, A.; Polovtseva, E. R.; Richard, C.; Smith, M. A. H.; Starikova, E.; Sung, K.; Tashkun, S.; Tennyson, J.; Toon, G. C.; Tyuterev, V. G.; Wagner, G. *J. Quant. Spectrosc. Radiat. Transfer* **2013**, *130*, 4−50.

(24) (a) Radney, J. G.; Bazargan, M. H.; Wright, M. E.; Atkinson, D. B. *Aerosol Sci. Technol.* **2009**, *43*, 71−80. (b) Brem, B. T.; Mena Gonzalez, F. C.; Meyers, S. R.; Bond, T. C.; Rood, M. J. *Aerosol Sci. Technol.* **2011**, *46*, 178−190. (c) Cappa, C. D.; Lack, D. A.; Burkholder, J. B.; Ravishankara, A. R. *Aerosol Sci. Technol.* **2008**, *42*, 1022−1032. (d) Flores, J. M.; Trainic, M.; Borrmann, S.; Rudich, Y. *Phys. Chem. Chem. Phys.* **2009**, *11*, 7943−7950. (e) Garvey, D. M.; Pinnick, R. G. *Aerosol Sci. Technol.* **1983**, *2*, 477−488. (f) Lang-Yona, N.; Rudich, Y.; Segre, E.; Dinar, E.; Abo-Riziq, A. *Anal. Chem.* **2009**, *81*, 1762−1769. (g) Presser, C. *J. Quant. Spectrosc. Radiat. Transfer* **2012**, *113*, 607−623. (h) Presser, C.; Conny, J. M.; Nazarian, A. *Aerosol Sci. Technol.* **2014**, *48*, 515−529. (i) Sedlacek, A.; Lee, J. *Aerosol Sci. Technol.* **2007**, *41*, 1089−1101. (j) Washenfelder, R. A.; Flores, J. M.; Brock, C. A.; Brown, S. S.; Rudich, Y. *Atmos. Meas. Technol.* **2013**, *6*, 861−877.

(25) (a) Radney, J. G.; Ma, X.; Gillis, K. A.; Zachariah, M. R.; Hodges, J. T.; Zangmeister, C. D. *Anal. Chem.* **2013**, *85*, 8319−8325. (b) Radney, J. G.; You, R.; Ma, X.; Conny, J. M.; Zachariah, M. R.; Hodges, J. T.; Zangmeister, C. D. *Environ. Sci. Technol.* **2014**, *48*, 3169−3176.

(26) NIST Technical Disclaimer: Certain commercial equipment, instruments, or materials (or suppliers, or software, ...) are identified in this paper to foster understanding. Such identification does not imply recommendation or endorsement by the National Institute of Standards and Technology, nor does it imply that the materials or equipment identified are necessarily the best available for the purpose.

(27) Santoro, R. J.; Semerjian, H. G.; Dobbins, R. A. *Combust. Flame* **1983**, *51*, 203−218.

DOI: 10.1021/acs.analchem.5b01541
Anal. Chem. 2015, 87, 7356−7363

(28) Shillings, A. J. L.; Ball, S. M.; Barber, M. J.; Tennyson, J.; Jones, R. L. *Atmos. Chem. Phys.* **2011**, *11*, 4273−4287.
(29) Zarzana, K. J.; Cappa, C. D.; Tolbert, M. A. *Aerosol Sci. Technol.* **2014**, *48*, 1133−1144.
(30) (a) Nguyen, T. B.; Lee, P. B.; Updyke, K. M.; Bones, D. L.; Laskin, J.; Laskin, A.; Nizkorodov, S. A. *J. Geophys. Res.: Atmos.* **2012**, *117*, D01207. (b) Powelson, M. H.; Espelien, B. M.; Hawkins, L. N.; Galloway, M. M.; De Haan, D. O. *Environ. Sci. Technol.* **2013**, *48*, 985−993. (c) Sareen, N.; Moussa, S. G.; McNeill, V. F. *J. Phys. Chem. A* **2013**, *117*, 2987−2996. (d) Updyke, K. M.; Nguyen, T. B.; Nizkorodov, S. A. *Atmos. Environ.* **2012**, *63*, 22−31.
(31) Bond, T. C.; Doherty, S. J.; Fahey, D. W.; Forster, P. M.; Berntsen, T.; DeAngelo, B. J.; Flanner, M. G.; Ghan, S.; Kärcher, B.; Koch, D.; Kinne, S.; Kondo, Y.; Quinn, P. K.; Sarofim, M. C.; Schultz, M. G.; Schulz, M.; Venkataraman, C.; Zhang, H.; Zhang, S.; Bellouin, N.; Guttikunda, S. K.; Hopke, P. K.; Jacobson, M. Z.; Kaiser, J. W.; Klimont, Z.; Lohmann, U.; Schwarz, J. P.; Shindell, D.; Storelvmo, T.; Warren, S. G.; Zender, C. S. *J. Geophys. Res.: Atmos.* **2013**, *118*, 5380−5552.
(32) Bond, T. C.; Bergstrom, R. W. *Aerosol Sci. Technol.* **2006**, *40*, 27−67.
(33) Lack, D. A.; Cappa, C. D. *Atmos. Chem. Phys.* **2010**, *10*, 4207−4220.
(34) Liu, C.; Panetta, R. L.; Yang, P. *Aerosol Sci. Technol.* **2011**, *46*, 31−43.
(35) (a) Arnott, W. P.; Moosmüller, H.; Sheridan, P. J.; Ogren, J. A.; Raspet, R.; Slaton, W. V.; Hand, J. L.; Kreidenweis, S. M.; Collett, J. L. *J. Geophys. Res.: Atmos.* **2003**, *108*, AAC 15-1−AAC 15-11. (b) Langridge, J. M.; Richardson, M. S.; Lack, D. A.; Brock, C. A.; Murphy, D. M. *Aerosol Sci. Technol.* **2013**, *47*, 1163−1173. (c) Lewis, K. A.; Arnott, W. P.; Moosmüller, H.; Chakrabarty, R. K.; Carrico, C. M.; Kreidenweis, S. M.; Day, D. E.; Malm, W. C.; Laskin, A.; Jimenez, J. L.; Ulbrich, I. M.; Huffman, J. A.; Onasch, T. B.; Trimborn, A.; Liu, L.; Mishchenko, M. I. *Atmos. Chem. Phys.* **2009**, *9*, 8949−8966.
(36) (a) Raspet, R.; Slaton, W. V.; Arnott, W. P.; Moosmüller, H. *J. Atmos. Oceanic Technol.* **2003**, *20*, 685−695. (b) Raspet, R.; Hickey, C. J.; Sabatier, J. M. *J. Acoust. Soc. Am.* **1999**, *105*, 65−73.

DOI: 10.1021/acs.analchem.5b01541
Anal. Chem. 2015, 87, 7356−7363